XL CILAMCE
IBERO-LATIN AMERICAN CONGRESS ON COMPUTATIONAL METHODS IN ENGINEERING
NOVEMBER 11-14, 2019
Praiamar Natal Hotel & Convention
Natal, RN-BRAZIL

# A SIMPLIFIED NUMERICAL APPROACH TO EVALUATION OF RESIDUAL SHAFT FRICTION IN DRILLED SHAFTS

**Augusto Bopsin Borges**
*augusto.borges@ufrgs.br*
*Federal University of Rio Grande do Sul*
*Av. Osvaldo Aranha, 99, 3$^{rd}$ floor - CEMACOM, 900.35-190, Rio Grande do Sul, Brazil*
**Renato Vaz Linn**
*renato.linn@ufrgs.br*
*Federal University of Rio Grande do Sul*
*Av. Osvaldo Aranha, 99, 4$^{th}$ floor - DEG UFRGS, 900.35-190, Rio Grande do Sul, Brazil*
**Fernando Schnaid**
*fernando@ufrgs.br*
*Federal University of Rio Grande do Sul*
*Av. Osvaldo Aranha, 99, ground floor - LEGG, 900.35-190, Rio Grande do Sul, Brazil*
**Samir Maghous**
*samir.maghous@ufrgs.br*
*Federal University of Rio Grande do Sul*
*Av. Osvaldo Aranha, 99, 3$^{rd}$ floor - CEMACOM, 900.35-190, Rio Grande do Sul, Brazil*

**Abstract.** Interpretation procedures of load-tests on instrumented piles rely conventionally upon measurements of strains assuming the instant immediately before starting the test as reference configuration for strains measures. Some experimental evidence shows that concrete in drilled shafts undergoes strains induced by the curing process comparable in magnitude to the strains measured during the load-tests. It is therefore expected that mobilization of shaft friction takes place before the load-test. Several authors have performed experimental and numerical analyses aiming to quantify the influence of those pre-load-test concrete volumetric strains on the measured bearing capacity using different approaches. The present work aimed to establish a reference framework for the existing and future works on this topic. In order to assess the influence of concrete strains induced by curing process on the shaft friction before the start of the load-tests in drilled shafts, several finite element numerical simulations are performed, considering the thermal, autogenous and drying strains. The analyses consider concrete as an isotropic linear-elastic material and the soil as an elastic-plastic material using the Mohr-Coulomb constitutive model natively implemented in the software ABAQUS. The results are interpreted focusing on the relevancy on the bearing capacity and load distribution along drilled shafts considering or not the strains induced by concrete curing.

**Keywords:** Residual stresses, Numerical modeling, Design parameters, Concrete curing, Drilled shafts

## 1 Introduction

The consideration of shaft friction mobilized during the installation of driven piles, prior to load-test procedures, is a well-known issue in foundation engineering (e.g. Rieke and Crowser [1]). For drilled shafts, however, many factors are still being evaluated In the context of drilled shafts, variations of normal stresses as well as associated mobilized shaft friction at the pile-soil interface, prior to external load application, are still being evaluated and should be also properly evaluated (Fellenius [2]). These distributions are expected to be influenced by concrete volumetric shrinkage or expansion strains that takes place in the pre-load-test phase.

Measurements during preload stage of instrumented drilled shafts in load-tests revealed significant variations in the strain profile, which would alter the reference configuration for the instrumentation zero readings (Leung et al. [3], Pennington [4], Viggiani and Vinale [5]). Those experimental results emphasize that the concrete undergoes significant volumetric shrinkage strains in a pre-load-test phase.

It comes from the above experimentally based works that the concrete curing phenomena can be viewed as an important component of pile-soil interaction, thus affecting the mechanical state in the soil around the pile.

Concerning the available shaft resistance in drilled shafts, rational procedures for its evaluation in granular soils are classically based on the assumption that the shaft friction mobilized at the pile-soil interface follows the Coulomb's linear friction model. In a simplified framework in which the geostatic state of stresses is preserved, the shaft friction at any depth $z$ along the pile-soil interface may be expressed as:

$$\tau\left(z\right)=\sigma_{h}^{\prime}\tan\,\delta\left(z\right)=K_{s}\left(z\right)\sigma_{v0}^{\prime}\left(z\right)\tan\,\delta\left(z\right)=\beta\left(z\right)\sigma_{v0}^{\prime}\left(z\right), \tag{1}$$

where $\tau$ is the unit shaft friction, $\sigma_{h}^{\prime}$ is the acting effective horizontal stress, $\delta$ is the interface friction angle, $\sigma_{v0}^{\prime}$ is the effective initial vertical stress, $K_{s}=\tau/(\sigma_{v0}^{\prime}\tan\,\delta)\;=\sigma_{h}^{\prime}/\sigma_{v0}^{\prime}$ is a measure of the acting lateral earth pressure, and $\beta=\tau/\sigma_{v0}^{\prime}\;=K_{s}\tan\,\delta$ is a shaft friction design parameter.

Although this assumption might be questionable from the mechanical viewpoint, Burland [6] highlighted that this expression represents a simple and logical starting point for this purpose due to the fact it is related to well-known soil mechanical properties.

Parameters $K_{s}\left(z\right)$ and $\beta\left(z\right)$ seek to encompass in a global manner the essential soil characteristics and consequent uncertainties in the evaluation of available shaft resistance. This formulation takes implicitly into account the stress history of the soil, mobilized friction angle and pile-soil interface properties, grain-size distribution, as well as changes in lateral stresses induced by pile installation procedures and strains at the pile-soil interface cause by concrete curing process.

Some authors seek to relate experimental evidences in the behavior of $K_{s}$ and $K_{0}$ with depth attributing it mainly to stress history. Kulhawy [7], to illustrate the importance given to stress history and related $K_{0}$ profile in determining $K_{s}$, considers that if overconsolidation is disregarded at shallow depths, the respective $\beta$ (and $K_{s}$) profiles would be constant with depth, and the main influent factor on the increase of $K_{s}$ at shallow depth should precisely be the preexisting $K_{0}$ profile.

The mobilized interface friction angle $\delta\left(z\right)$ has been the subject of several studies pointing out its dependence on the pile-soil interface roughness. Typical $\delta\left(z\right)$ values range from the critical state friction angle $\phi_{crit}^{\prime}$ for smoothed interfaces to the peak friction angle $\phi_{peak}^{\prime}$ for rough interfaces. Drilled shafts always exhibit high roughness at the pile-soil interface and failure yielding is likely to occur in the soil mass, following a simple shear mode governed by $\phi_{crit}^{\prime}$ angle.

According to Kulhawy [8] and Kulhawy [7], the typical profiles with values of $\beta$ and $K_{s}$ decreasing with depth can be explained as reflecting the reduction in $K_{0}$ with depth, together with the decrease in soil friction angle as confining stresses increase.

Focusing the analyses on the effects induced on the shaft friction of floating drilled shafts embedded in granular soils, in the pre-load-test stage, Mascarucci [9] and Mascarucci et al. [10]) performed axisymmetric numerical simulations in axially load piles considering curing strains coupled with evolving

stiffness during the curing process. Both approaches used the standard finite-difference FLAC 2D software with a strain softening behavior for the interface constitutive model and a *Strain Softening Model* for the soil. These studies emphasized that restarting the strain measurements in instrumented piles immediately before the load-test would introduce significant errors in the distribution of shaft friction along the pile-soil interface.

Based on a simplified but consistent formulation, the present work aims at presenting a reference framework for existing and future numerical analyses on this topic. Restricting the subsequent analysis to concrete drilled shaft embedded in granular soils, this work focuses on the effects induced on the shaft friction by concrete curing strains during pre-load-test stage. In that respect, the analysis is undertaken in the context of fully drained conditions, not considering pore pressure effects.

## 2 Numerical Model

As the problem of cylindrical piles axially loaded in homogeneous soil (usual configuration for drilled shafts) complies with the revolution symmetry with respect to the pile axis, axisymmetric modeling was adopted for the analyses. Dimensions of the model in terms of the pile length $L$ and pile diameter $D$, together with model boundary conditions are shown in Fig. 1. The different zones in Fig. 1 were established for mesh control and refinement. The typical finite element model discretization used is shown in Fig. 2. Four-node axisymmetric quadrilateral elements with bilinear displacement CAX4, available in the ABAQUS finite element library, were used for both pile and soil. Due to the high roughness observed along drilled pile shaft (Loukidis and Salgado [11]), resulting from drilling and casting concrete processes, a perfect bonding condition is assumed at the pile-soil interface (rough tangential contact). Further detailed information about the modeling is available in Borges [12].

The width and height are respectively fixed as $B = 25D$ and $H = 2.5L$ for the geometric model, according to standard discretization used in foundation analyses (Randolph and Wroth [13]). The concrete was modeled as an isotropic linear-elastic material (Young's modulus $E_c$ = 30 GPa and Poisson's ratio $\nu_c$ = 0.2), while the behavior of the homogeneous soil is described by means of an elasto-plastic Mohr-Coulomb model, with Young's modulus $E_s$ = 50 MPa, Poisson's ratio $\nu_s$ = 0.2, friction angle $\phi$ = 29° and dilatancy angle $\psi$ = 1°. Physical material properties of Ottawa sand defined in Han et al. [14] as speficic gravity $G_s$ = 2.65, minimum void ratio $e_{min}$ = 0.48 and maximum void ratio $e_{max}$ = 0.78 were used. The coefficient of earth pressure at rest is fixed to $K_0$ = 0.4.

A convergence analysis was performed to define the finite element mesh configuration, comparing the results of the model with those presented by Han et al. [14] for a 300 mm diameter and 10 m long pile. Dry sand conditions were assumed, with relative density $I_D$ = 50%, corresponding to a void ratio $e$ = 0.63 and an effective specific weight $\gamma'$ = 15.95 kN/m$^3$ (density $d$ = 1,625.77 kg/m$^3$). The same density was used for both soil material and pile concrete in all subsequent analyses.

The numerical simulations, including the validation analysis, were performed in three steps (Fig. 3): *geostatic* step, in which the dead load is applied by acceleration of gravity $g$ = 9.81 m/s$^2$ using an automatic time increment scheme under small deformations conditions; *curing_process* step, for pile thermal volumetric strains, imposed following FIB [15] model recommendations; and *load_test* step, in which a prescribed displacement of $w = 10\%D$ is incrementally applied.

For numerical validation and convergence analysis, the concrete curing process was disconsidered. Comparison of model predictions obtained herein and results from Han et al. [14] are shown in Fig. 4. The numerical values for ultimate total ($Q_{ult}$), lateral ($Q_{l,ult}$) and base ($Q_{b,ult}$) resistances are presented in Table 1. The agreement observed between the present simulations and results provided in Han et al. [14] validates the proposed modeling.

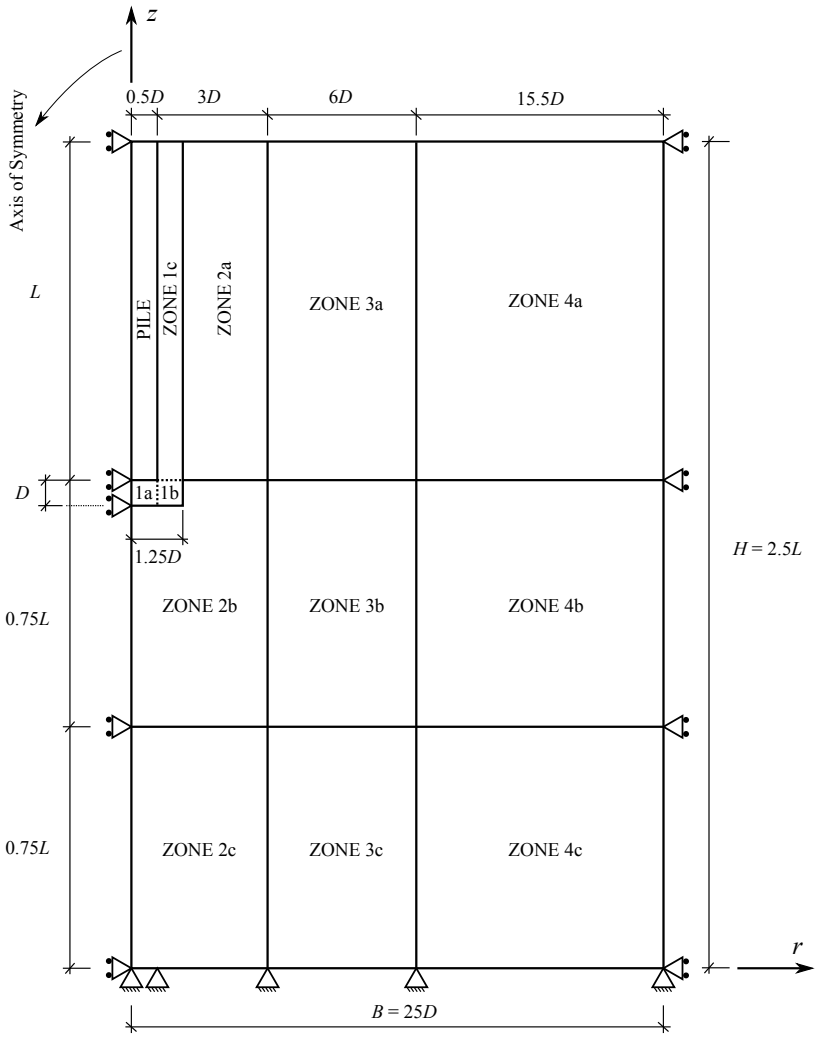


Figure 1. Global dimensions and boundary conditions in *r*–*z* plane

Table 1. Ultimate total, lateral and base resistances ($w/D$ = 10%)

| Resistance component | Present work | Han et al. [14] |
|---|---|---|
| $Q_{ult}$ (kN) | 463.85 | 454.93 |
| $Q_{l,ult}$ (kN) | 352.57 | 359.49 |
| $Q_{b,ult}$ (kN) | 114.80 | 96.19 |

## 3 Numerical assessment of residual shaft friction

A series of finite element simulations to investigate the effects of concrete curing on the mobilized shaft friction of drilled shafts were performed. Keeping the pile length fixed to $L$ = 20 m, the effects of the pile slenderness $L/D$ were investigated taking pile diameters in the range of 0.5 m to 1.5 m ($L/D$ ranging from 40 to 13.33) for both dry ($S$ = 0) and saturated ($S$ = 1) sand conditions. Appropriate effective specific unit weight of $\gamma'$ = 15.95 kN/m$^3$ ($d$ = 1,625.77 kg/m$^3$) and $\gamma'$ = 9.93 kN/m$^3$ ($d$ = 1,012.27 kg/m$^3$) were respectively adopted for the dry ad saturated conditions. General characteristics of the numerical finite element discretization used in each configuration are summarized in Table 2.

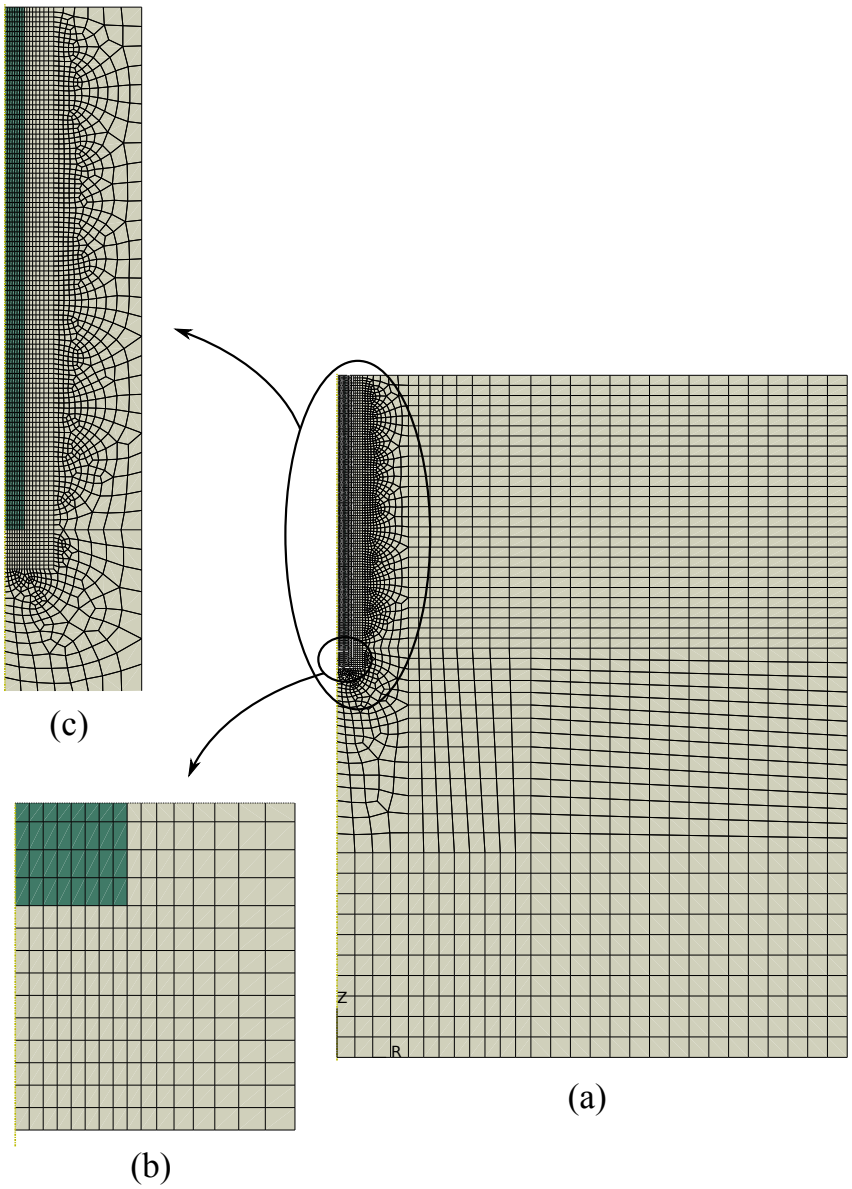


Figure 2. Finite element mesh used for model geometry (a), detailed mesh at pile base (b) and detailed mesh at pile shaft (c)

Table 2. Numerical finite element discretization used in the analyses

| Analysis | $S$ | Pile Diameter | $L/D$ | Number of elements - soil | Number of elements - pile |
|---|---|---|---|---|---|
| SIM-01 | 0% | 0.50 m | 40 | 9,676 | 2,560 |
| SIM-02 | 100% | | | | |
| SIM-03 | 0% | 1.0 m | 20 | 4,880 | 1,280 |
| SIM-04 | 100% | | | | |
| SIM-05 | 0% | 1.50 m | 13.33 | 3,359 | 856 |
| SIM-06 | 100% | | | | |

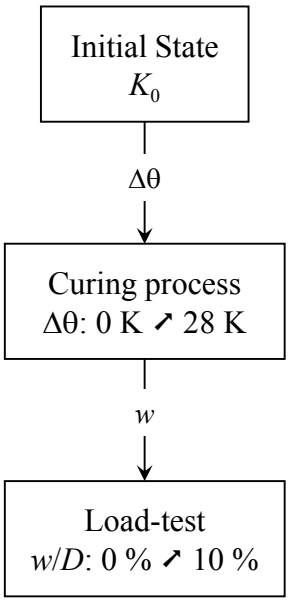


Figure 3. General scheme of the analyses

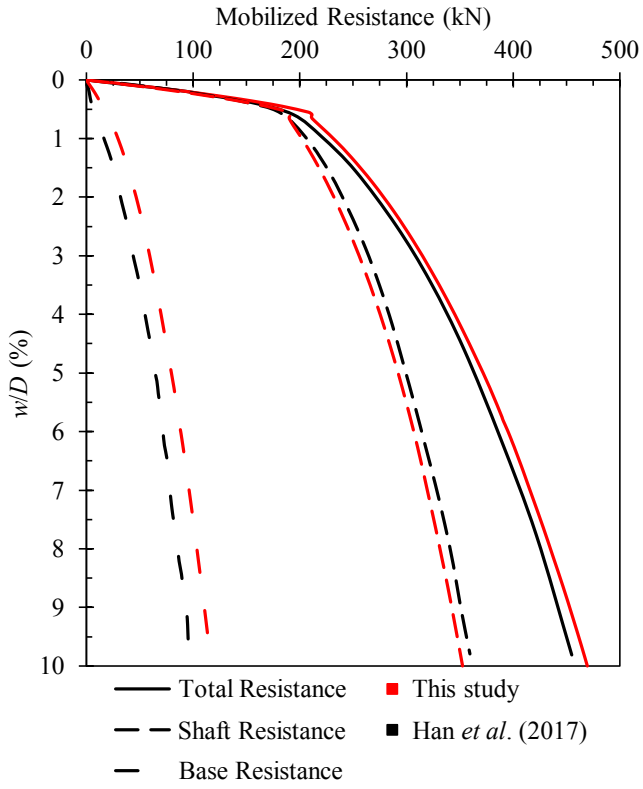


Figure 4. Results for the mobilized resistance as a function of the relative settlement of the pile head - comparison between Han et al. [14] and the present work

### 3.1 Simulation of concrete curing process

Due to microstructural mechanisms, concrete shrinkage is classically separated into autogenous and drying shrinkage (e.g. FIB [15], Holt [16]). Hydration of the cement compounds involves mainly exothermic reactions that raise the temperature of the concrete mass, inducing thermal volumetric strains. The total volumetric strains resulting from the concrete curing process $\varepsilon_{cs}$ is a sum of those three strain components (Eq. (2)): autogenous shrinkage $\varepsilon_{cas}$, drying shrinkage $\varepsilon_{cds}$, and thermal shrinkage $\varepsilon_{th}$.

$$\varepsilon_{cs} = \varepsilon_{cas} + \varepsilon_{cds} + \varepsilon_{th} \tag{2}$$

The development of the autogenous and drying shrinkage during the curing period of 28 days was calculated following FIB [15] model recommendations. In the model, these components are computed using the concrete compressive strength as a design parameter accounting at macroscopic scale for concrete strength class, aggregate type, cross-section geometry, relative humidity and duration of drying. The thermal shrinkage resulting from a temperature change $\Delta\theta$ induced by the curing process is calculated from concrete thermal expansion, with a thermal expansion coefficient $\alpha_c = 10 \times 10^{-6}$ K$^{-1}$, as (Mehta and Monteiro [17]):

$$\varepsilon_{th} = \alpha_c \Delta\theta, \tag{3}$$

where $\Delta\theta \in [0\text{ K}, 28\text{ K}]$ is considered in the analysis.

The distribution of temperature variation raising in concrete during curing varies with depth and is heteronomous within the cross-section of the pile. For simplicity, a spatially uniform temperature profile was assumed, and the temperature profile measured in a drilled shaft by Pennington [4] was used here for the entire pile (Fig. 5). The temperature is assumed to remain constant after 20 days.

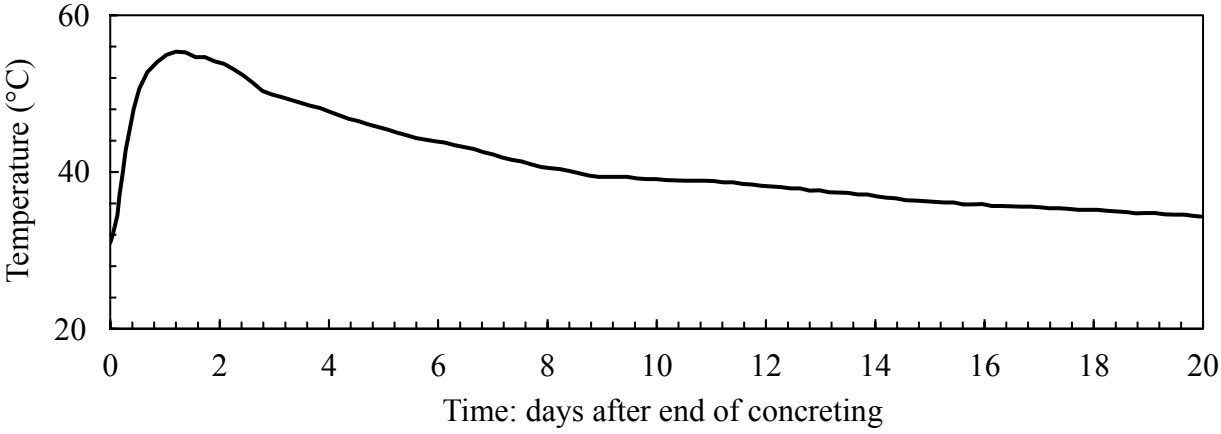


Figure 5. Experimental profile of temperature change with time (Pennington [4])

In the thermal analysis it is assumed that concrete sets at maximum temperature, so that the development of differential strains between the contracting pile and the soil can be estimated from this reference time. Strains due to the thermal expansion of the pile before the maximum temperature are not accounted, as well as associated loading that would be transferred to the adjacent soil.

In the numerical simulation of the curing process, the evolution of the strains in the concrete is imposed in the *curing_process* step and the temperature change $\Delta\theta$ was used as a kinematic time for assessing the mechanical state of the system, since material properties can be expressed as a function of temperature through a thermo-mechanical coupling. To meet the model of thermal strains, together with the autogenous and drying shrinkage proposed in FIB [15] recommendations, the curing strains that are actually imposed to the pile are evaluated considering an appropriate *fictitious* and discrete non-linear coefficient of expansion for each $\Delta\theta \in [0\text{ K}, 28\text{ K}]$, superimposing the strain components (Eq. (2)). By a selection of the results, given that variations in the pile slenderness $L/D$ showed small influence in the overall results, only the results of analyses SIM-01 and SIM-02 will be presented. Figure 6 displays the curing strains imposed following the above indicated procedure.

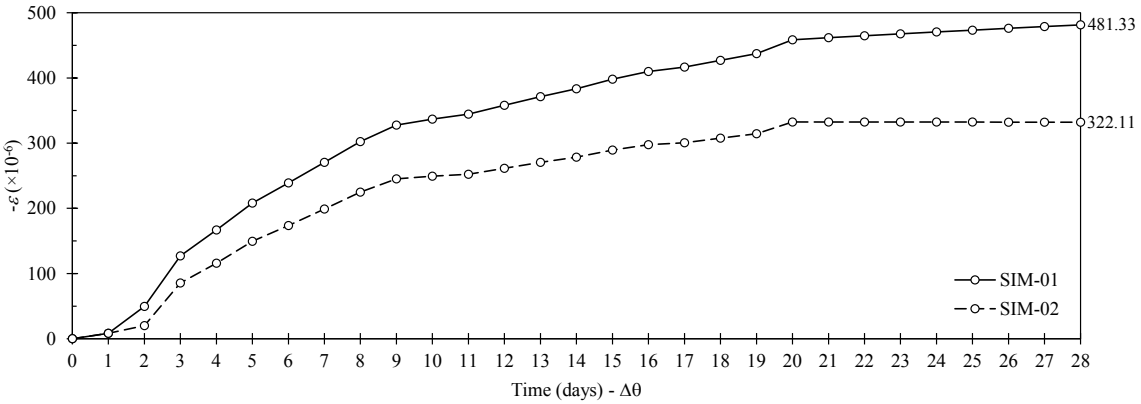


Figure 6. Imposed curing strains in the *curing_process* step

## 4 Results and discussion

In the *load_test* step a total displacement of $10\%D$ (often assumed a representative of ultimate state in foundation design) was prescribed at the pile head, linearly applied during the time step, after completion of the *curing_process*, when it is applicable. Numerical simulations were performed with and without accounting for the curing process for each selected slenderness and saturation condition.

The mobilized shaft friction $\tau$ along the depth obtained for SIM-01 and SIM-02 are presented in Fig. 7, corresponding to the ultimate pile load obtained for $10\%D$ total displacement. Solid lines represent simulations accounting for concrete curing and dashed lines stands for simulation disregarding this process by suppressing the *curing_process* step. $\tau_{real}$ refers to shaft friction computed from the initial reference configuration when concrete curing starts, while $\tau_{virtual}$ is computed considering as the reference configuration the configuration reached after completion of the curing process (immediately before the start of the load-test). A measure of the deviation between $\tau_{real}$ and $\tau_{virtual}$ can be introducted as:

$$\tau_r = \tau_{real} - \tau_{virtual}, \tag{4}$$

which represents the error $\tau_r$ introduced when volumetric concrete curing strains are not considered.

It is relevant to note the fact that the actual distribution in shaft friction $\tau_{real}$ at ultimate state coincides with the values calculated when the curing process is disregarded. That is consistent with general theorems of plasticity stating that stress field at ultimate state is insensitive to initial stress distribution state (Halphen and Salençon [18], Salençon [19]). Figure 7 emphasize that significant error can be induced when the unit shaft friction is evaluated based on the so-called virtual reference configuration.

The volumetric strains in the pile due to the curing induce contraction in the intire pile, resulting in downward relative movements in the upper part of the pile and upward relative movements in its lower part. These relative movements between the contracting pile and the adherent soil elements mobilize shaft friction in the soil elements (positive upwards and negative downwards). The results from Fig. 7 demonstrate that "zeroing" the instruments at the start of a load test may reveal mechanically inconsistent for shaft friction analysis.

In order to observe the impact of the concrete curing strains on the total load distribution along the pile at ultimate state, normalized load distribution curves are shown in Fig. 8 for analyses SIM-01 and SIM-02. In Fig. 8 it can be observed that, although the normalized load distribution computed from both real and virtual conditions differ along the shaft, the corresponding values of base resistance are close to each other. It implies that the predicted ultimate shaft and base load components are not affected by the procedure conventionally adopted by taking the reference configuration as the time immediately before starting a load test.

Going back to unit shaft friction analysis, the pile equilibrium expressed under *real* and *virtual* conditions respectively can be written as:

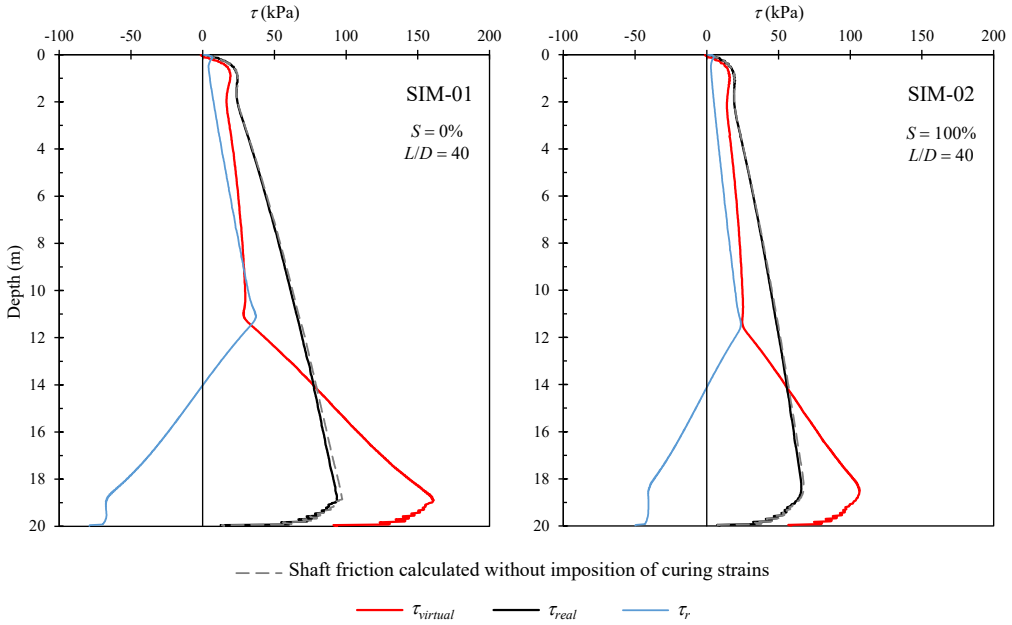


Figure 7. Distribution of unit shaft friction on soil elements adjacent to the pile for 10%$D$ total displacement and $L/D$ = 40 (SIM-01 and SIM-02)

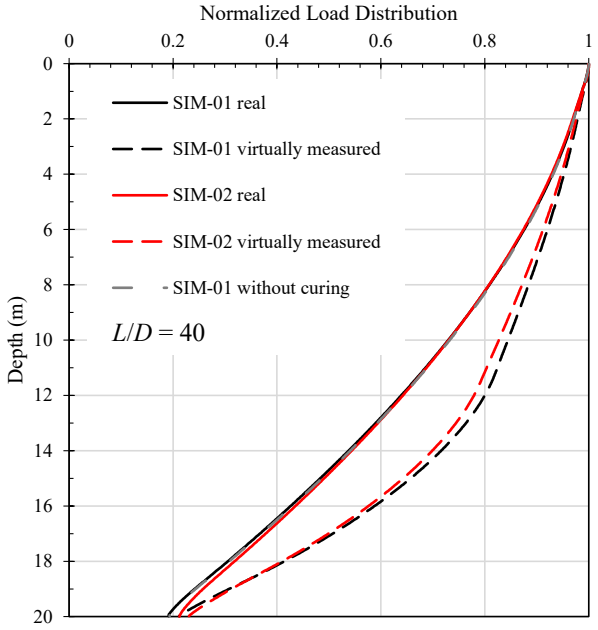


Figure 8. Normalized load distribution curves for 20 m long non-displacement drilled shafts for analysis with $L/D$ = 40 (SIM-01 and SIM-02)

$$\int_0^L \tau_{real} dz + Q_b^{real} = \gamma_c L, \tag{5}$$

$$\int_0^L \tau_{virtual} dz + Q_b^{virtual} = \gamma_c L, \tag{6}$$

where $Q_b^{real}$ and $Q_b^{virtual}$ are the resistance base computed for real and virtual conditions, respectively.

Combining the above Eq. (5) and Eq. (6), and observing that $\Delta Q_b = Q_b^{real} - Q_b^{virtual} \approx 0$, yield

$$\int_0^L \tau_r dz = -\Delta Q_b \approx 0. \tag{7}$$

Equation 7 indicate that the distribution of $\tau_r$ shall always exhibit a neutral point with change in signal. The location of this neutral point depends on soil and pile parameters. In homogenous soils, as considered in the present analysis, the neutral point approximately lies at a depth of $z$ = 2/3$L$, which is in accordance with previous numerical works by Mascarucci [9] and Mascarucci et al. [10].

Numerical predictions for distributions of $\tau_r$ and $\tau_{virtual}$ are in agreement with experimental data measured from instrumented piles (e.g. Altaee et al. [20], Pereira [21], Vesić [22]), showing that $\tau_{virtual}$ distribution along depth can significantly differ from the actual $\tau$ distribution, although both yield the same bearing capacity of the pile.

The calculated load-displacement curves for each case are presented in Fig. 9 with and without considerations of the curing process and associated pre-load-step strains.

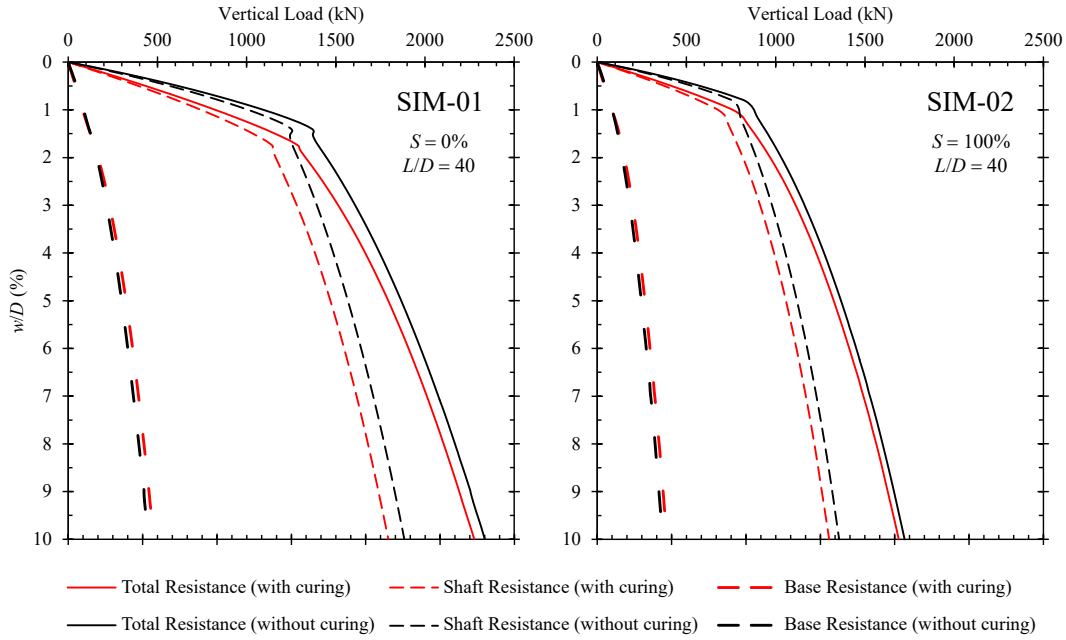


Figure 9. Load-settlement curves for 20 m long drilled shafts for analyses with $L/D$ = 40 (SIM-01 and SIM-02)

It can be noted from Fig. 9 that the consideration of curing strains has little effect on the ultimate load $Q_{ult}$ distribution. The results summarized in Table 3 - where *w/c* stands for 'with curing' - are in accordance with limit analysis theory (Salençon [19]), as already mentioned when discussing unit shaft friction distribution.

Table 3. Results for the analyses at $w/D$ = 10%

| Analysis | $Q_{l,w/c}$ (kN) | $Q_{l,w/c}/Q_l$ | $Q_{b,w/c}$ (kN) | $Q_b/Q_{b,w/c}$ | $Q_{ult,w/c}$ (kN) | $Q_{ult,w/c}/Q_{ult}$ |
|---|---|---|---|---|---|---|
| SIM-01 | 1,794.37 | 95.24% | 481.47 | 93.74% | 2,275.85 | 97.45% |
| SIM-02 | 1,299.62 | 95.88% | 389.57 | 94.14% | 1,689.18 | 98.08% |

This set of results demonstrates that curing strains slightly affect the ultimate state design of drilled

shafts. However, this phenomenon is expected to influence the shaft friction distribution and bearing load–strain behavior at earlier stages, such as loads controlling serviceability limit state.

## 5 Influence of concrete curing on design parameters

The influence of concrete curing on the $K_s$ and $\beta$, which control the distribution of shaft friction in conventional pile design (see Eq. (1)), has been evaluated by mean of numerical simulations with consideration for the *virtual* and *real* cases. The obtained $K_s$ profiles are shown in Fig. 10 and computed for an interface friction angle $\delta = \phi = 29°$. It should be recalled that perfect bonding condition at the pile-soil interfaced has been assumed throughout the paper. The distribution of coefficient $\beta$ can be directly deduced from $K_s$ since the soil profile is considered homogeneous with constant interface friction angle ($\beta = K_s \tan\delta$).

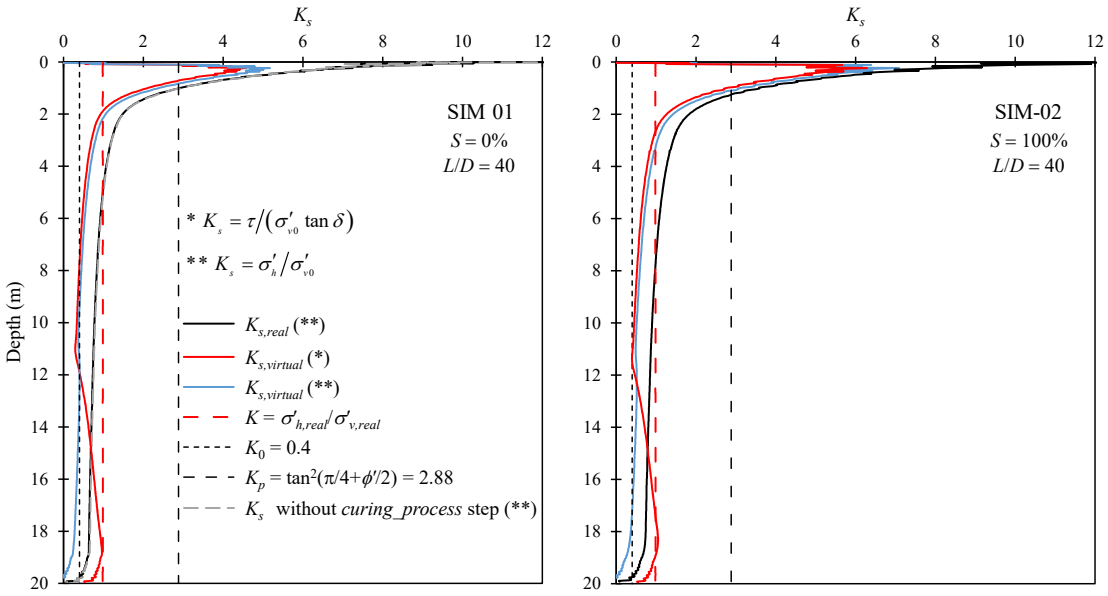


Figure 10. $K_s$ distribution along pile shaft

Referring to Fig. 10, the following comments may be made to guide engineering design of drilled shafts:

- The singularity associated with the high values of $K_s$ computed in the upper soil layers is reflecting vanishing vertical stresses in this region and, therefore, not necessarily indicates a overconsolidation at shallow depths.
- Disregarding this upper crust, the values of $K_s$ exhibit a slight reduction with depth and rapidly tends to a constant value.
- Coefficients $K_{s,real}$ and $K_{s,virtual}$ show close profiles and are marginally higher that $K_0$ value.
- For the two limiting saturation conditions ($S$ = 0% and $S$ = 100%) evaluated in this paper, it is found from the numerical simulations that saturation has qualitatively similar effects on $K_s$ than $L/D$.

## 6 Conclusions

Although it is widely accepted that load-tests performed at relatively large prescribed displacements to reach the ultimate limit state is the most reliable procedure to analyze the behavior of piles, technological factors such the method of construction and reference configuration are expected to affect the measured response.

Based on these premises, numerical analyses were performed to assess the effect of curing process on the shaft friction regarded as a major parameter in pile design. The numerical analyses indicate that

ultimate resistance is in fact not significantly affected by the curing process-imposed strains. The same trend is observed for base and lateral mobilized resistances.

The volumetric strains in the pile due to the curing are likely to induce contraction in the whole pile, generating downward relative movements in the upper part of the pile and upward relative movements in its lower part. This phenomenon explains the errors that can be introduced by "zeroing" the instruments immediately before starting a pile load-test.

Regarding pile analysis and design, the distribution of the stress parameter $K_s$ along the pile shaft, classically used to evaluate ultimate shaft friction profile, is not significantly affected by concrete curing, saturation conditions in homogeneous soils.

## Acknowledgements

The authors wish to express their appreciation to CAPES and CNPq for the support provided to the research group.

## References

[1] Rieke, R. D. & Crowser, J. C., 1987. Interpretation of Pile Load Test Considering Residual Stresses. *Journal of Geotechnical Engineering*, vol. 113, n. 4, pp. 320–334.

[2] Fellenius, B. H., 2017. *Basics of Foundation Design Basics of Foundation Design*. Pile Buck International, Inc., Vero Beach.

[3] Leung, C. F., Radhakrishnan, R., & Wong, Y. K., 1988. Observations of an instrumented pile-raft foundation in weak rock. *Proceedings of the Institution of Civil Engineers*, vol. 84, n. 4, pp. 693–711.

[4] Pennington, D. S., 1995. Cracked? Exploring post construction evidence in the interpretation of trial pile data. *Proceedings of the Institution of Civil Engineers - Geotechnical Engineering*, vol. 113, n. 3, pp. 132–143.

[5] Viggiani, C. & Vinale, F., 1983. Comportamento di pali trivellati di grande diametro in terreni piroclastici. *Rivista Italiana di Geotecnica*, vol. 2, pp. 59–84.

[6] Burland, J. B., 1973. Shaft friction of piles in clay. *Ground Engineering*, vol. 6, n. 3, pp. 30–42.

[7] Kulhawy, F. H., 1991. Drilled Shaft Foundations. In *Foundation Engineering Handbook SE - 14*, chapter 14, pp. 537–552. Springer US, Boston, MA.

[8] Kulhawy, F. H., 1984. Limiting tip and side resistance - Fact or fallacy. In *Analysis and Design of Pile Foundations*, pp. 80–98, New York, N.Y. American Society of Civil Engineers.

[9] Mascarucci, Y., 2012. *Un nuovo approccio per la valutazione della resistenza laterale dei pali trivellati in terreni sabbiosi*. PhD thesis, La Sapienza, Roma.

[10] Mascarucci, Y., Mandolini, A., & Miliziano, S., 2013. Effects of residual stresses on shaft friction of bored cast in situ piles in sand. *Journal of Geo-Engineering Sciences*, vol. 1, pp. 37–51.

[11] Loukidis, D. & Salgado, R., 2008. Analysis of the shaft resistance of non-displacement piles in sand. *Géotechnique*, vol. 58, n. 4, pp. 283–296.

[12] Borges, A. B., 2019. *Análise dos Efeitos das Tensões Residuais em Estacas Escavadas: abordagem computacional*. Master thesis, Federal University of Rio Grande do Sul.

[13] Randolph, M. F. & Wroth, C. P., 1978. Analysis of Deformation of Vertically Loaded Piles. *Journal of the Geotechnical Engineering Division*, vol. 104, n. 12, pp. 1465–1488.

[14] Han, F., Salgado, R., Prezzi, M., & Lim, J., 2017. Shaft and base resistance of non-displacement piles in sand. *Computers and Geotechnics*, vol. 83, pp. 184–197.

[15] FIB, 2012. Model Code 2010. In *FIB Model Code for Concrete Structures 2010*. Ernst & Sohn.

[16] Holt, E. E., 2001. Early age autogenous shrinkage of concrete. *VTT Publications*, , n. 446, pp. 2–184.

[17] Mehta, P. K. & Monteiro, P. J. M., 2006. *Concrete - Microstructure, Properties, and Materials*. McGraw-Hill, 3rd. edition.

[18] Halphen, B. & Salençon, J., 1987. *Élastoplasticité*. Presses de l'École Nationale des Ponts et Chaussées, Paris.

[19] Salençon, J., 1983. *Calcul à la rupture et analyse limite*. Presses de l'École Nationale des Ponts et Chaussées, Paris.

[20] Altaee, A. A., Evgin, E., & Fellenius, B. H., 1993. Load transfer for piles in sand and the critical depth. *Canadian Geotechnical Journal*, vol. 30, n. 3, pp. 455–463.

[21] Pereira, T. A. B. P., 2012. *Análise e Dimensionamento de Estacas Sujeitas a Compressão Axial. Aplicações na Região Administrativa Especial de Macau*. Master thesis, Universidade do Porto.

[22] Vesić, A. S., 1970. Tests on instrumented piles - Ogeechee River site. *Journal of Soil Mechanics and Foundation Engineering Division*, vol. 96, n. SM2, pp. 561–584.